http://dx.doi.org/10.5012/bkcs.2012.33.10.3407

Improved Photolysis of Water from Ti Incorporated Double Perovskite Sr_2FeNbO_6 Lattice

P. H. Borse, C. R. Cho,‡ S. M. Yu,† J. H. Yoon,† T. E. Hong,† J. S. Bae,† E. D. Jeong,† and H. G. Kim†,*

Solar H_2 PEC Laboratory, International Advanced Research Center for Powder Metallurgy and New Materials (ARC International), Balapur PO, Hyderabad, AP 500 005, India
†Division of High Technology Materials Research, Korea Basic Science Institute, Busan 609-735, Korea
**E-mail: hhgkim@kbsi.re.kr*
‡Department of Nano Fusion Technology, Pusan National University, Pusan 609-735, Korea
Received April 26, 2012, Accepted July 26, 2012

The Ti incorporation at Fe-site in the double perovskite lattice of Sr_2FeNbO_6 (SFNO) system is studied. The Ti concentration optimization yielded an efficient photocatalyst. At an optimum composition of Ti as x = 0.07 in $Sr_2Fe_{1-x}Ti_xNbO_6$, the photocatalyst exhibited 2 times the quantum yield for photolysis of H_2O in presence of CH_3OH, than its undoped counterpart under visible light ($\lambda \geq 420$ nm). Heavily Ti-doped $Sr_2Fe_{1-x}Ti_xNbO_6$ lattice exhibited poor photochemical properties due to the existence of constituent impurity phases as observed in the structural characterization, as well as deteriorated optical absorption. The higher electron-density acquired by *n*-type doping seem to be responsible for the more efficient charge separation in $Sr_2Fe_{1-x}Ti_xNbO_6$ ($0.05 < x < 0.4$) and thus consequently displays higher photocatalytic activity. The Ti incorporated structure also found to yield stable photocatalyst.

Key Words : Photocatalysts, Sr_2FeNbO_6, Visible light, Photocatalytic activity, H_2 evolution

Introduction

The need of environmentally digestible energy generating materials is inducing tremendous interest in exploration of iron-containing oxide photocatalysts.[1-3] Sr_2FeNbO_6 (SFNO) is one such oldest known system that falls under the category of potential photocatalyst for energy generation.[3] The Fe-containing oxide effectively renders the desired visible light absorption property to the photocatalyst due to the existence of Fe-d bands.[3] However, the electrical properties are equally important to improve the photocatalytic performance of an intrinsic semiconductor. There are no reports on the study of dopant induced photocatalytic property enhancement in case of SFNO. The present report describes our work on the doping of Ti in SFNO double perovskite lattice.

It is known that *n*-type materials exhibit efficient photocatalytic properties due to their well suited band energetics, enhanced exciton radius, and subsequent electron-hole charge separation. Doping of Ti^{4+} at Fe-site is expected to yield an electron rich material by virtue of extra valence electrons in the crystal lattice. As per reports in past the substitution of larger valence metal-ion (Ti^{4+}) sub at lower valency site (Fe^{3+}) yields *n*-type material thereby yielding high photocurrent and photocatalytic hydrogen generation in a photocatalytic reaction.[4,5] We report here that Ti-doping in SFNO lattice enhances the photocatalytic activity of the host lattice. Such approach to produce an efficient energy material has been an important topic in photocatalysis research. Specifically, materials for solar hydrogen production by water splitting should possess high-standard optoelectric properties, in addition to the suitable band energetics and posses durability in aqueous solutions. The tunability of the physico-chemical properties of photocatalyst by virtue of their size and shape renders a wider applicability of such nanostructured materials. TiO_2 has been known for its wide applicability in photocatalysis research.[6,7] Yet, it suffers from the UV absorbing ability due to its large band gap of more than 3.2 eV. Currently the field of visible light water splitting photocatalyst is being nurtured by various kinds of conventional and new single component materials (CdS, WO_3, Fe_2O_3, TaON, *etc*) as well as composite materials.[8-11] However nanostructured materials have great potential in this area.

There have been several reports on the binary,[12,13] ternary metal oxides,[19-22,14-16] composite metal oxides, and modified nanocomposites[17,18] to tackle the problem of efficiency and stability improvement of photocatalysts. However the doping induced improvement in the physical and electrical properties lends a major advantage in development of efficient photocatalysts. Thus special emphasis has been given on exploring and on improvement of the electronic, structural and chemical properties of the related materials. In the present report, we have attempted to alter the electrical property of double-perovskite structure of SFNO, which in turn improves its photocatalytic activity.

Experimental

$Sr_2Fe_{1-x}Ti_xNbO_6$ ($0.05 < x < 0.4$) photocatalyst were synthesized by using the conventional solid state reaction (SSR) method. For the preparation of $Sr_2Fe_{1-x}Ti_xNbO_6$ ($0.05 < x <$

0.4) sample of various Ti doping concentrations, the stoichiometric amounts of TiO_2 (99.9%, Aldrich) and Sr_2CO_3 (99.5%, Aldrich), Fe_2O_3 (99%, Aldrich) and Nb_2O_5 (99.9%, Aldrich) were mixed and ground in methanol. The pelletized powders were calcined at 600-1200 °C for 5 h in static furnace. On the other hand, for the purpose of comparison, $TiO_{2-x}N_x$ particle was also prepared by the hydrolytic synthesis method (HSM).[19] In this synthesis, an aqueous ammonium-hydroxide solution with an ammonia content of 28-30% (99.99%, Aldrich) was added drop by drop to titanium (III)-chloride (20%) solution ($TiCl_3$, Kanto, and containing 0.01% iron as the major impurity) for 30 min under N_2 flow in an ice bath while continuously stirring. Later, the suspension was further stirred for 5 h to complete the reaction. After completion of the reaction, the precipitate was filtered in air and washed several times with deionized water. The filtered powder was dried at 70 °C for 3-4 h in a convection oven. The sample obtained at this stage was an amorphous powder containing ammonia and titanium species. Further, this sample was calcined at 400 °C for 2 h in air flow in an electric furnace. This yielded the desirable crystalline $TiO_{2-x}N_x$ powder.

The $Sr_2Fe_{1-x}Ti_xNbO_6$ ($0.05 < x < 0.4$) samples were characterized by using an X-ray diffractometer (Mac Science Co., M18XHF). X-ray diffraction (XRD) results were compared with the Joint Committee Powder Diffraction Standards (JCPDS) data for phase identification. The optical properties, mainly the band gap energies of the as-prepared materials, were estimated by using an UV-Visible diffuse reflectance spectrometer (Shimadzu, UV 2401). The particulate morphology was characterized by using scanning electron microscopy (SEM, Hitachi, S-2460N). A detailed structural characterization was carried out by using high-resolution transmission electron microscopy (HR-TEM, Philips, CM 200).

The X-ray photoelectron spectroscopy (XPS) study was performed with a Thermo Fisher Scientific Inc. Theta Probe XPS system (UK) with a base pressure of 4×10^{-10} mbar (UHV), using monochromatized Al Kα X-ray source (hν = 1486.6 eV) with charge compensation at KBSI (Busan, Korea). Emitted photoelectrons were detected by a multichannel detector at a take off angle of 90° relative to the sample surface. Survey spectra were obtained at a resolution of 1 eV, and high-resolution spectra were acquired at a resolution of 0.1 eV. The all obtained binding energy (BE) were determined with the C1s core level peak at 284.6 eV as a reference.

For all the samples, the photo-reduction of water was carried out at room temperature in an upper-irradiation type Pyrex reaction vessel hooked up into a closed gas circulation system. Photocatalytic reduction was carried out by irradiating suspended powders using Xe-arc lamp (450W-Oriel) equipped with a cutoff filter ($\lambda \geq 420$ nm). The H_2 evolution was examined in an aqueous methanol solution (distilled water 70 mL and CH_3OH 30 mL) by stirring 0.3 g of the catalyst loaded with 0.2 wt % Pt. Before photocatalytic reactions, all the catalysts were loaded with 0.2 wt % Pt by using conventional impregnation method using aqueous $PtCl_2$. The concentration of the reaction product (H_2) was determined by a gas chromatograph equipped with a thermal conductivity detector (a molecular sieve 5-Å column and Ar carrier)

Results and Discussion

Figure 1 shows the XRD patterns of the Ti incorporated samples *i.e.* $Sr_2Fe_{1-x}Ti_xNbO_6$ ($0.05 < x < 0.1$) made by sintering the powders at 1200 °C/ 5 hr. In undoped SFNO *i.e.* $x = 0$, a highly crystalline phase was identified. Undoped and all the doped samples exhibited a cubic double perovskite Sr_2FeNbO_6 crystal structure belonging to *Pm-3 m* (lattice constant a = 3.97 Å) space group. There was no detectable impurity phase formed in any of the samples within the present low Ti doping concentration. However, it is important to note that there is difference is atomic size of Ti and Fe ions that can have a distortive effect on the unit cell of SFNO and thus discussed below. Accordingly a careful investigation of main (101) plane of cubic Sr_2FeNbO_6 was carried out and region wise spectrum is shown in the Figure 2 for each

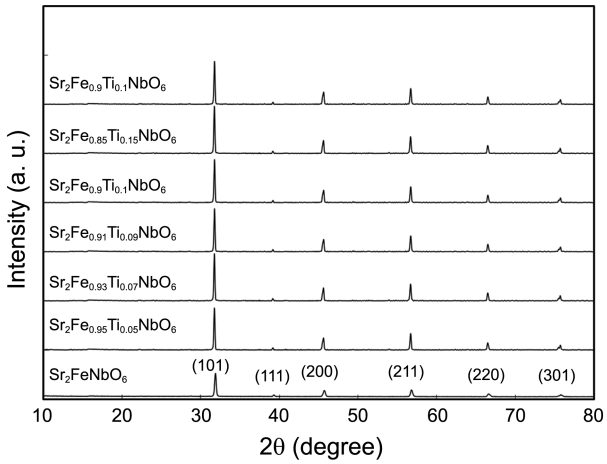

Figure 1. XRD patterns for the $Sr_2Fe_{1-x}Ti_xNbO_6$ for x = 0, 0.05 to 0.1 samples sintered at 1200 °C for 5 h.

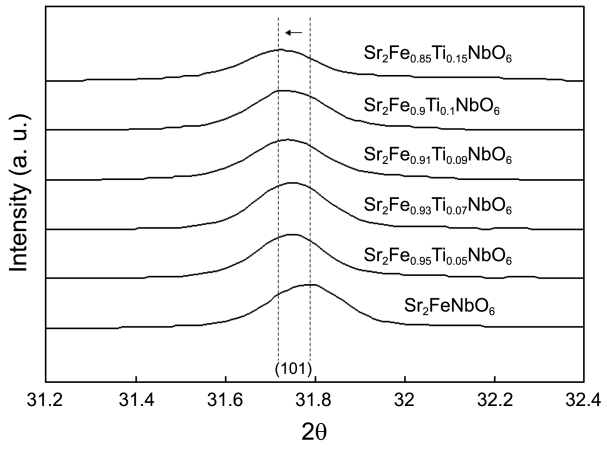

Figure 2. Ti-doping induced shift in the 2θ value for the 101 plane of cubic Sr_2FeNbO_6 as deduced from XRD of $Sr_2Fe_{1-x}Ti_xNbO_6$ for $x \sim 0$, 0.05 to 0.15.

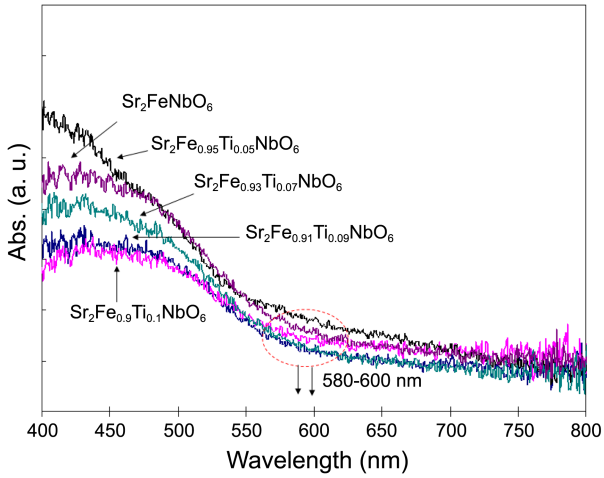

Figure 3. UV-Vis diffuse reflectance spectra of $Sr_2Fe_{1-x}Ti_xNbO_6$ for x ~ 0, 0.05, 0.07, and 0.09.

sample. The (101) peak shows a distinct shift in diffraction angle with an increase in the Ti doping concentration, thus indicating planer distortion for the $Sr_2Fe_{1-x}Ti_xNbO_6$ cubic lattice. The $Sr_2Fe_{0.95}Ti_{0.05}NbO_6$ lattice showed notable peak

Table 1. Visible light photocatalytic activities for H_2 and O_2 evolution respectively from water-methanol mixtures and silver nitrate solutions over $Sr_2Fe_{1-x}Ti_xNbO_6$ ($0.05 < x < 0.4$) photocatalysts and $TiO_{2-x}N_x$

Catalyst[b]	Band gap energy		H_2 evolution		O_2 evolution	
	E_g (eV)	λ (nm)	μmol/h	QY[a]	μmol/h	QY[a]
Sr_2FeNbO_6	2.06	600	13.5	1.68	580	36.7
$Sr_2Fe_{0.95}Ti_{0.05}NbO_6$	2.13	580	19.2	2.4	591	38.4
$Sr_2Fe_{0.93}Ti_{0.07}NbO_6$	2.13	580	28.5	3.5	650	41.1
$Sr_2Fe_{0.91}Ti_{0.09}NbO_6$	2.13	580	15.7	1.9	600	39.1
$Sr_2Fe_{0.9}Ti_{0.1}NbO_6$	2.13	580	11.5	1.4	570	37.1
$Sr_2Fe_{0.85}Ti_{0.15}NbO_6$	2.13	580	10.6	1.3	550	35.8
$Sr_2Fe_{0.8}Ti_{0.2}NbO_6$	2.13	580	8.6	1.0	310	20.2
$Sr_2Fe_{0.7}Ti_{0.3}NbO_6$	2.13	580	5.4	0.6	244	15.9
$Sr_2Fe_{0.6}Ti_{0.4}NbO_6$	2.13	580	2.7	0.3	140	9.1
$PbBi_2Nb_2O_9$	2.88	431	7.6	0.95	518	29.6
$TiO_{2-x}N_x$	2.73	451	Trace	0	227	14.8

[a]QY-quantim yield (estimated as per Ref. 27, 28). [b]Catalyst loaded with 0.2 wt % Pt; 0.3 g; Light source, 450 Watt, Xe-Arc lamp (Oriel) in inner irradiation quartz cell with UV cut-off filter (λ ≥ 420 nm). Photo-reduction reaction was performed in aqueous CH_3OH solution [CH_3OH (30 mL) + distilled water (70 mL)]

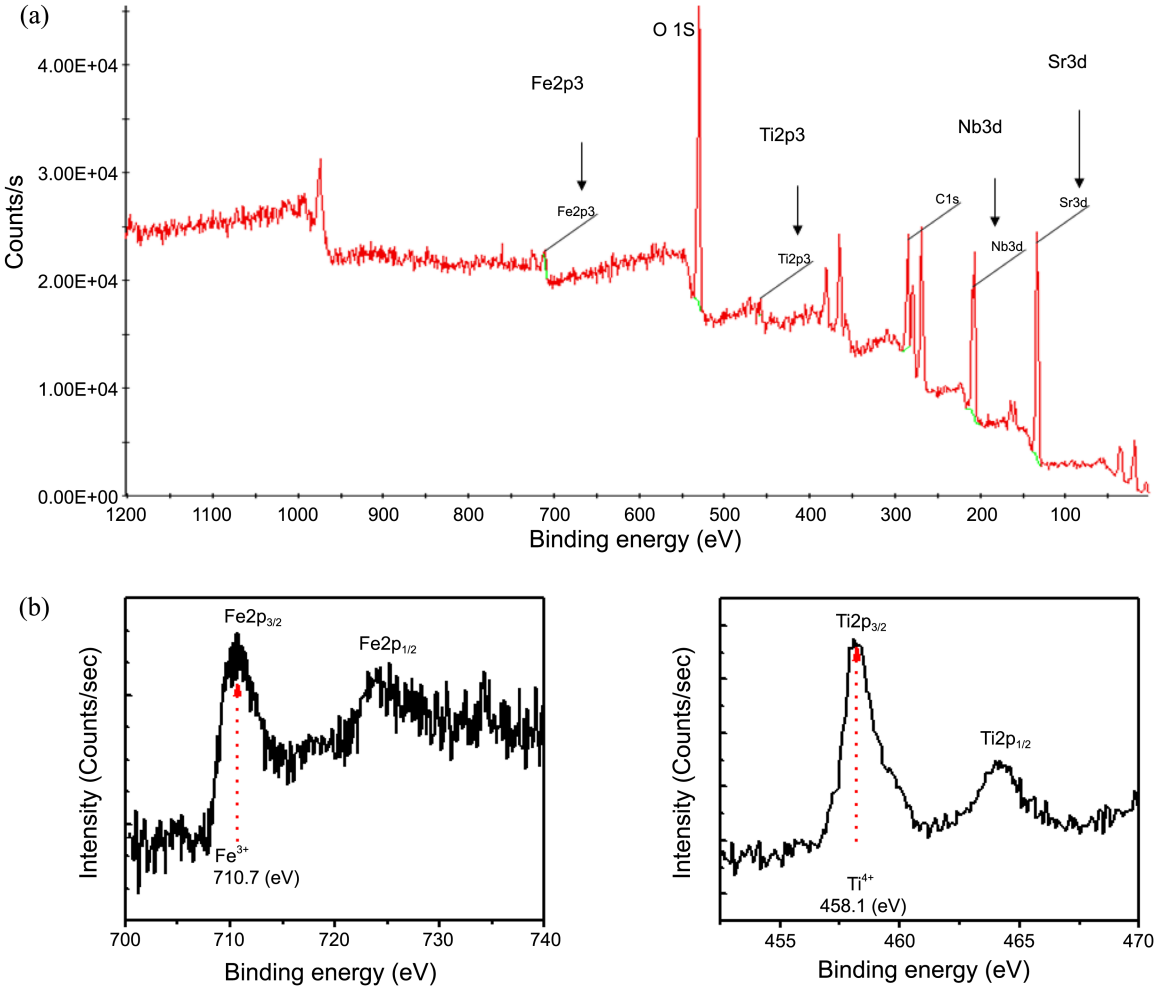

Figure 4. XPS survey scan, alongwith the region wise core-level spectra of titanium (Ti 2p) and iron (Fe 2p) for $Sr_2Fe_{0.93}Ti_{0.07}NbO_6$ sample studied to validate the dopant oxidation states.

shift with respect to undoped sample. It can be further noted that there is a concentration-dependent decrease in the diffraction angle (for 101 plane) of Sr_2FeNbO_6. This decrease is expected due to the difference in the ionic radii of Fe^{+3} (0.64 nm) and Ti^{+4} (0.68 nm) at octahedral site of the host lattice. Such difference is bound to induce a lattice distortive effect, but without destroying the original host lattice. Thus Figure 2 clearly demonstrates this effect for the case of Ti doping of $x < 0.15$. This also thus validates the doping of the Ti in the SFNO lattice.

Figure 3 shows the UV-DRS spectra for $Sr_2Fe_{1-x}Ti_xNbO_6$ with $x = 0$ and $x = 0.1$ indicating the change in band-gap of the doped SFNO. Estimated band gaps of doped and undoped sample are presented in Table 1 in later part of the text. All the samples showed an absorption onset in the range of $\lambda = 580$-600 nm indicating the band gap of doped SFNO lie at 2.13 eV. Thus Ti-doping is found to alter the bulk band-gap of host lattice but in a rather less significant manner.

XPS measurements were carried out to identify the oxidation state of Fe-ion in $Sr_2Fe_{0.93}Ti_{0.07}NbO_6$ photocatalyst. Figure 4(a) shows the XPS survey spectrum of $Sr_2Fe_{0.93}Ti_{0.07}NbO_6$ sample, indicating the existence of Sr, Ti, Nb, O, and Fe elements. This is confirmed by the observation of the photoelectron peaks appearing at respective binding energies of Sr 3d, Ti 2p3/2, O 1s, Nb 3d alongwith a weak photo-electron peak at 710.7 eV (Fe 2p3/2). Figure 4(b) displays the core level spectra of the Fe 2p3/2 revealing that the peak at 710.7 eV is symmetrical and thus Fe-ion can be ascribed to the trivalent oxidation state (Fe^{3+}). Thus the XPS study validates the trivalent oxidation state of dopant.

Owing to the favorable optical and electronic properties, the visible light photocatalyst are expected to generate photocurrents due to photogenerated charge carriers. Figure 5 validates that aqueous suspension of $Sr_2Fe_{0.93}Ti_{0.07}NbO_6$, Sr_2FeNbO_6 and N-doped TiO_2, containing acetate (donor) and Fe^{3+} (acceptor) generated the photocurrents under visible light irradiation. It shows that $Sr_2Fe_{0.93}Ti_{0.07}NbO_6$ generated 1.5 times higher photocurrent than the undoped counterpart demonstrating that Ti doping play an important role in yielding higher photocurrent due to larger charge carrier produced. On the contrary the N-doped TiO_2 showed no photocurrent under given illumination and other electro-chemical conditions.

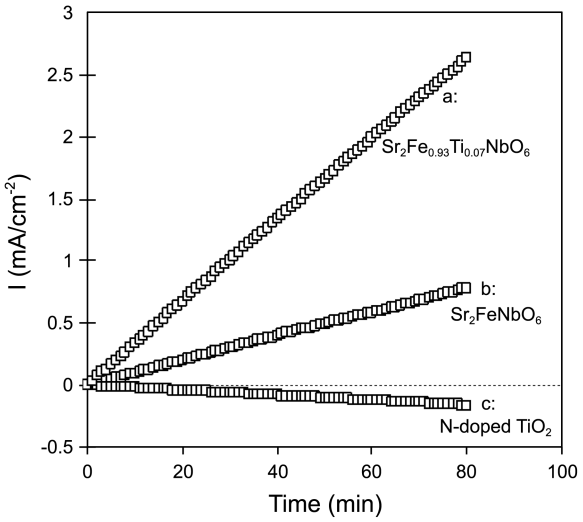

Figure 5. The generated photocurrents under 420 nm wavelngth (visible light) for (a) $Sr_2Fe_{0.93}Ti_{0.07}NbO_6$, (b) Sr_2FeNbO_6 and (c) N-doped TiO_2 material suspensions with acetate and Fe^{3+} as an electron donors or acceptor respectively. Experimental conditions Photocatalyst = 25 mg in 75 mL; acetate (0.1 M); Fe^{3+} (0.1 mM); continuous N_2 purging; pH = 1.4; E_{app} = 0.6 V (*vs* SCE); Pt plate (10 × 10 × 0.125 mm), Pt gauge as working and counter electrode respectively.

Figure 6(a) shows the SEM micrograph of $Sr_2Fe_{0.93}Ti_{0.07}NbO_6$ sample, alongwith the high resolution transmission micro-graph in Figure 6(b) of the particle surface of Pt impregnated sample. The micron sized grains are clearly visible from the study. The HRTEM image of 0.2 wt % platinum-loaded $Sr_2Fe_{0.93}Ti_{0.07}NbO_6$ shows the well dispersed platinum particles (20 nm) on $Sr_2Fe_{0.93}Ti_{0.07}NbO_6$. This indicates that the platinum is mostly deposited on the outer surface of the $Sr_2Fe_{0.93}Ti_{0.07}NbO_6$ sample.

We evaluated the photocatalytic activities of the $Sr_2Fe_{0.93}Ti_{0.07}NbO_6$ material for hydrogen production from water splitting. Table 1 shows the estimated photocatalytic H_2 evolution for doped and undoped SFNO samples, along with $TiO_{2x}N_x$ sample. It is noteworthy that all these samples were loaded with Pt, prior to the photocatalytic H_2 pro-duction from a methanol-water solution, as discussed above. The Pt loading over the photocatalyst substrate facilitates efficient electron transfer to electrolyte and produce hydro-gen during the $2H^+ + 2e^- \rightarrow H^2$ reaction at the conduction band of the photocatalyst. Table 1 shows the summary of results of photo-reduction reaction over the samples in a methanol-water mixture. Doped samples showed an enhanced H_2 generation whereas $TiO_{2-x}N_x$ sample showed trace amount of H_2 evolution. It can be found that the $Sr_2Fe_{0.93}Ti_{0.07}NbO_6$ yields maximum H_2 evolution. The photocatalyst stability and time dependent H_2 evolution can be seen in Figure 7. The figure clearly demonstrates photocatalytic hydrogen generation from these samples. The evolution rate increased with the reaction time, the H_2 evolution regained after evacuation of reactor indicating the photocatalytic nature of the reaction.

The quantum yield (QY) for the photocatalysts of the

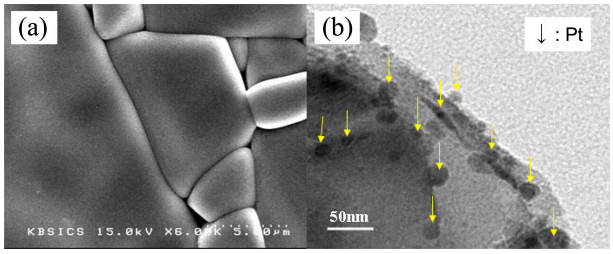

Figure 6. (a) SEM micrograph of $SrFe_{0.93}Ti_{0.07}NbO_6$ and its TEM image (b) showing the loaded Pt particle over base photocatalyst. Pt was deposited on photocatalysts by photodeposition method under visible light ($\lambda \geq 420$ nm).

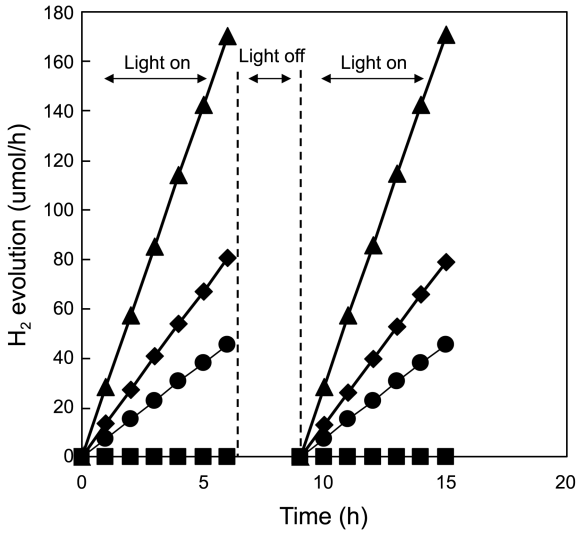

Figure 7. Time course of H_2 gas evolution from ▲: $Sr_2Fe_{0.93}Ti_{0.07}NbO_6$, ◆: Sr_2FeNbO_6, ●: $PbBi_2Nb_2O_9$, ■: $TiO_{2-x}N_x$ under visible light irradiation in an aqueous solution by stirring 0.3 g of catalyst loaded with Pt(0.2 wt %). The reaction system was evacuated every 6 h in order to remove gaseous products from the gas phase.

material was calculated using the following the equation:[20]

$$\mathrm{QY} = \frac{Rate(H_2\ evolution)}{12.639} \times \frac{[(I_1-I_3)-(I_1-I_2)]\cdot A_1}{A_2} \times 100$$

where I_1 is the blank light intensity, I_2 is the scattered light intensity, I_3 is the photocatalyst light intensity, A_1 is the illuminated area of the photo reactor, A_2 is area of the sensor, and 12.639 is the mole number of photons with $\lambda \geq 420$ nm emitted from the lamp during 1 h. The estimated QYs of the undoped, doped SFNO and the $TiO_{2-x}N_x$ photocatalyst shown in Table 1 indicate that optimum Ti doped sample *i.e.* $Sr_2Fe_{0.93}Ti_{0.07}NbO_6$ is more efficient photocatalyst for photo reduction reaction. In order to investigate the stability of the photocatalyst samples under photocatalytic reaction conditions, we checked the structure of $Sr_2Fe_{0.93}Ti_{0.07}NbO_6$ before and after photocatalytic reaction. The structure and the crystalline state of $Sr_2Fe_{0.93}Ti_{0.07}NbO_6$ before and after reaction were almost the same, as demonstrated in Figure 8. Thus, $Sr_2Fe_{0.93}Ti_{0.07}NbO_6$ crystals prepared by the solid state reaction method are very stable under visible light and in the aqueous medium.

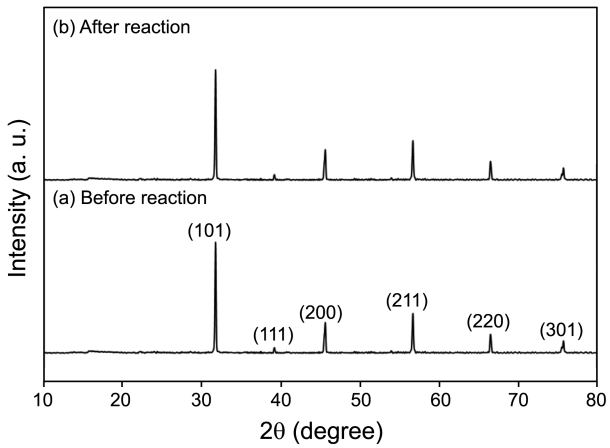

Figure 8. XRD patterns of Pt(0.2 wt %)/$Sr_2Fe_{0.93}Ti_{0.07}NbO_6$ (a) before and (b) after photocatalytic reaction under visible light irradiation.

The correlation of the physico-chemical properties of doped and undoped SFNO indicates that the electron rich $Sr_2Fe_{0.93}Ti_{0.07}NbO_6$ yields higher activity than undoped SFNO. This can be correlated to the effect of the dopant concentration, which consequently plays a vital role in controlling the thickness (W) of space charge layer as described by following equation:[21]

$$W = [2\, E\varepsilon_0 V_s / eN_D\,]^{1/2},$$

where E and ε_0 are respectively the static dielectric constants of semiconductor and vacuum, V_s the surface potential, N_D (donor concentration) and e as electron charge. It can be recalled[4] that a higher electron density of donor-rich semiconductors would create a narrower charge depletion region (as implied by above equation) at semiconductor/electrolyte interface thus resulting in an increased band bending. This will lead to an efficient electron-hole separation and ultimately to the higher photocatalytic QYs in donor-rich semiconductor photocatalysts as demonstrated in the present work. The lowering of QYs above an optimum donor concentration possibly comes from the formation of the impurity phase.

Conclusions

An efficient SFNO photocatalyst, is fabricated by doping of electron donor (Ti^{+4}) element in a spinel-crystal lattice in $Sr_2Fe_{1-x}Ti_xNbO_6$ ($0.05 < x < 0.4$). The material doped with electron donor (Ti^{+4}), $Sr_2Fe_{1-x}Ti_xNbO_6$ with an optimum composition of $x = 0.07$ exhibits an unchanged band gap, and generates 1.5 times higher photocurrent, and shows enhanced quantum yield (of upto 2%) for photodecomposition of methanol-water mixture, than undoped material under visible light ($\lambda \geq 420$ nm).

Acknowledgments. This work has been supported by a KBSI grant (C32223) and by the Hydrogen Energy R&D Center, Korea.

References

1. Kim, H. G.; Borse, P. H.; Jang, J. S.; Jeong, E. D.; Jung, O.; Suh, Y. J.; Lee, J. S. *Chem. Comm.* **2009**, 5889.
2. Jang, J. S.; Borse, P. H.; Lee, J. S.; Jung, O.; Cho, C. R.; Jeong, E. D.; Ha, M. G.; Won, M. S.; Kim, H. G. *Bull. Korean Chem. Soc.* **2009**, *30*, 1738.
3. Matsumoto, Y.; Omae, M.; Sugiyama, K.; Sato, E. *J. Phys. Chem.* **1987**, *91*, 577.
4. Kim, H. G.; Borse, P. H.; Jang, J. S.; Jeong, E. D.; Lee, J. S. *Mater. Lett.* **2008**, *62*, 1427.
5. Ishizawa, N.; Marumo, F.; Kawamura, T.; Kimura, M. *Acta Crystallogr. Sect. B* **1975**, *31*, 1912.

6. Hoffman, M. R.; Martin, S. T.; Choi, W.; Bahnemann, D. W. *Chem. Rev.* **1995**, *95*, 69.
7. Zong, X.; Yan, H.; Wu, G.; Ma, G.; Wen, F.; Wang, L.; Li, C. *J. Am. Chem. Soc.* **2008**, *130*, 7176.
8. De, G. C.; Roy, A. M.; Bhattacharya, S. S. *Int. J. Hydrogen Energy* **1996**, *21*, 19.
9. Hwang, D. W.; Kim, J.; Park, T. J.; Lee, J. S. *Catal. Lett.* **2002**, 80, 53.
10. Yamashita, H.; Takeuchi, M.; Kishiguchi, S. *J. Photochem. Photobiol. A* **2002**, *148*, 257.
11. Asahi, R.; Ohwaki, T.; Aoki, K.; Taga, Y. *Science* **2001**, *293*, 269.
12. Zhong, D. K.; Sun, J.; Inumaru, H.; Gamelin, D. R. *J. Am. Chem. Soc.* **2009**, *131*, 6086.
13. Formal, F. L.; Graetzel, M.; Sivula, K. *Adv. Func. Mater.* **2010**, *20*, 1099.
14. Yu, J.; Kudo, A. *Adv. Func. Mat.* **2006**, *16*, 2163.
15. Kim, H. G.; Hwang, D. W.; Lee, J. S. *J. Am. Chem. Soc.* **2004**, *126*, 8912.
16. Kim, H. G.; Borse, P. H.; Jang, J. S.; Ahn, C. W.; Jeong, E. D.; Lee, J. S. *Adv. Mater.* **2011**, *23*, 2088.
17. Kim, H. G.; Borse, P. H.; Choi, W.; Lee, J. S. *Angew. Chem. Int. Ed.* **2005**, *44*, 4585.
18. Sivula, K.; Formal, F. L.; Gratzel, M. *Chem. Mater.* **2009**, *21*, 2862.
19. Jang, J. S.; Kim, H. G.; Ji, S. M.; Bae, S. W.; Jung, J. H.; Shon, B. H.; Lee, J. S. *J. Solid State Chem.* **2006**, *179*, 1064.
20. Bae, S. W.; Borse, P. H.; Hong, S. J.; Jang, J. S.; Lee, J. S.; Jeong, E. D.; Hong, T. E.; Yoon, J. H.; Jin, J. S.; Kim, H. G. *J. Korean Phys. Soc.* **2007**, *51*, S22.
21. Schiavello, M.; Sclafani, A. In *Photocatalysis: Fundamentals & Applications*; Serpone, N., Pelizzetti, E., Eds.; Wiley Interscience: New York, 1989; p 170.